Journal of Power Sources 204 (2012) 127–132

Contents lists available at SciVerse ScienceDirect

Journal of Power Sources

journal homepage: www.elsevier.com/locate/jpowsour

Effect of nano $LiFePO_4$ coating on $LiMn_{1.5}Ni_{0.5}O_4$ 5 V cathode for lithium ion batteries

D. Liu [a], J. Trottier [a], P. Charest [a], J. Fréchette [a], A. Guerfi [a], A. Mauger [b], C.M. Julien [c], K. Zaghib [a,*]

[a] Institut de Recherche d'Hydro-Québec (IREQ), 1800 Bd Lionel Boulet, Varennes, QC, Canada J3X 1S1
[b] Université Pierre et Marie Curie-Paris-6, IMPMC, 4 place Jussieu, 75005 Paris, France
[c] Université Pierre et Marie Curie 6 Paris-6, PECSA, UMR 7195, Bat. F74, 4 place Jussieu, 75005 Paris, France

ARTICLE INFO

Article history:
Received 5 October 2011
Received in revised form
17 November 2011
Accepted 18 November 2011
Available online 20 December 2011

Keywords:
Lithium batteries
High-voltage cathodes
Spinel
Coating

ABSTRACT

C-$LiFePO_4$ nanoparticles were used as surface coating for the $LiMn_{1.5}Ni_{0.5}O_4$ spinel. However, it is impossible to prepare $LiFePO_4$-coated $LiMn_{1.5}Ni_{0.5}O_4$ by traditional sol–gel methods in Ar. Therefore, we used a new mechano-fusion dry process that provides a simple way to obtain surface coating for battery materials. Surface elemental analyses indicate that $LiFePO_4$ nanoparticles were not simply mixed with the $LiMn_{1.5}Ni_{0.5}O_4$, but successfully coated on its surface. This new composite was tested as a cathode for Li-ion batteries. $LiMn_{1.5}Ni_{0.5}O_4$ showed better capacity retention after $LiFePO_4$ coating, especially at high rate (>10*C*). After 100 cycles at 1*C*, the capacity declined from 105 to 65 mAh g^{-1} for the bare $LiMn_{1.5}Ni_{0.5}O_4$. In contrast, 82 mAh g^{-1} of capacity was still obtained for the $LiFePO_4$-coated $LiMn_{1.5}Ni_{0.5}O_4$ with 75% of capacity retention after 140 cycles under 1*C*. The results suggest that the improved performance is due to the improvement of the surface conductivity due to the carbon coated $LiFePO_4$ covering, end the protection against reactions of $LiMn_{1.5}Ni_{0.5}O_4$ with the electrolyte.

1. Introduction

Power/energy densities are critical parameters for successfully adopting the lithium ion battery technology for hybrid electric vehicle (HEV) and plug-in hybrid electric vehicle (PHEV) application. To increase the power/energy densities of lithium-ion battery, much attention has been given to the spinel $LiMn_{1.5}Ni_{0.5}O_4$ (LMN). Compared to the traditional 4 V $LiMn_2O_4$ spinel and layered $LiCoO_2$, or the 3.5 V olivine $LiFePO_4$ cathodes, LMN provides access to the Ni(IV) to Ni(II) formal valences at about 4.7 V versus lithium [1,2]. The access to two formal valence states of Ni without a significant step between them is possible because the Fermi energy ε_F is pinned at the top of the O-2p bands [3]. In addition, and at contrast with $LiMn_2O_4$, Mn remains in the Mn(IV) valence state in the lithiation/delithiation process, thus avoiding the presence of the Mn(III) Jahn–Teller ion that is responsible for local deformation and strains reducing the cycling life of the battery. However, ε_F is very close to the highest occupied molecular orbital (HOMO) of the carbonate electrolyte, so that a passivating solid/electrolyte-interface (SEI) layer is formed to obtain the reversible Ni(IV)/Ni(II) redox reaction [4,5]. The surface reactions between cathode/electrolyte have been confirmed to be one of the major reasons leading to the degradation in the electrochemical performance of the 4.7 V spinel [6]. In this regard, various metal oxides, carbon and phosphates [7–12] have been used as surface coatings to improve the electrochemical performance of the spinel LMN.

Meanwhile, after the pioneering work of Padhi et al. [13], $LiFePO_4$ (LFP) also has been extensively studied as a promising cathode candidate for lithium ion batteries due to its environmental compatibility, thermal stability, and low cost. Especially, nano-sized LFP with appropriate amount of carbon coating exhibits high-rate performance as well as long cycling life [14,15]. Nevertheless, only few studies focused on the LFP as a surface coating, except for $LiCoO_2$ [16] and $Li[Ni_{0.5}Co_{0.2}Mn_{0.3}]O_2$ [17]. In this work, we explored the effect of LFP as a coating for LMN. Two different routes have been explored, namely, the traditional sol-gel method, and the mechano-fusion dry process. The second one was successful to synthesize the LFP-coated LMN cathodes. The structures, surface morphology as well as the electrochemical performances were investigated.

2. Experimental

2.1. Synthetic procedure

First, the LFP-coated LMN was prepared by a traditional sol-gel method using citric acid as chelating agent and carbon source [18]. Stoichiometric amounts of ferrous oxalate dihydrate (99%,

* Corresponding author. Tel.: +1 450 652 8019; fax: +1 450 652 8424.
E-mail address: zaghib.karim@ireq.ca (K. Zaghib).

0378-7753/$ – see front matter © 2011 Elsevier B.V. All rights reserved.
doi:10.1016/j.jpowsour.2011.11.059

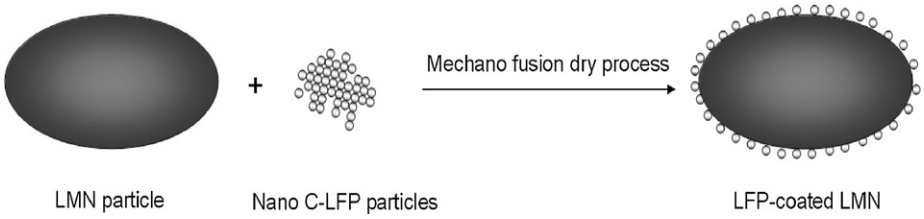

Fig. 1. Schematic illustration of the LFP-coated LMN by a mechano-fusion dry process, for which the commercial carbon-coated LFP serves as guest particles and LMN serves as host particles.

Alfa Aesar) and lithium hydroxide monohydrate (98%, Alfa Aesar) were dissolved in distilled water into which citric acid solution was added dropwise under stirring. To this solution, diammonium hydrogen phosphate (99%, Aldrich) was then added with continuous stirring. The molar ratio of citric acid to total metal ions was controlled to be 1:1. The solution was continually stirred during 1 h and then the appropriate amount of LMN powders (South Korea) was dispersed. The mixture was gently heated with continuous stirring for several days and then became the gel precursor. The gel precursor was heated at 700 °C (heating rate 5 °C per hour) in a tube furnace, and calcined for 12 h under Ar atmosphere before natural cooling down.

According to the other process, the LFP-coated LMN was also prepared by a new mechano-fusion dry process (illustrated in Fig. 1). In this process, commercial carbon-coated LFP (served as guest particles, particle size 100 nm, carbon content around 2 wt%) and LMN (served as host particles, South Korea) were directly dry milled for several minutes in a Mechano Fusion System (Hosokawa Micron Corp., Japan). The mass ratio of LFP to LMN was 20:80.

2.2. Structural and physical characterization

Powder X-ray diffraction (XRD) patterns were step-scan recorded on a Philips X'pert apparatus equipped with Cu Kα radiation in steps of 0.05° over the range $10 < 2\theta < 90°$ for each sample. Scanning electron microscopy (SEM) and transmission electron microscopy (TEM) images were obtained using an electronic microscope Hitachi model HD-2700 with 200 kV, 5 kV and 3 kV operating potential. The TEM samples were ultrasonically treated in a solution of isopropyl alcohol and then deposited on silica substrate. Near-surface elemental analyses were carried out by energy-dispersive X-ray spectroscopy (EDX).

2.3. Electrochemical studies

The electrochemical performance of each sample was evaluated with a standard CR2032 coin cell composed of a cathode, lithium anode, a Celgard polypropylene separator, and $LiPF_6$ in 1:1 ethylene carbonate/diethylene carbonate (EC/DEC) as electrolyte. The cathode was prepared by mixing 75 wt% oxide with 20 wt% acetylene black and 5 wt% polytetrafluoroethylene (PTFE) binder; the mixture was rolled into thin sheets that were punched into 1-cm-diameter circular discs. The typical electrode mass and thickness was in the range 4–8 mg and 0.02–0.06 mm, respectively. All the cells were fabricated in an argon-filled glove box and galvanostatically cycled with a VMP-cycler (Biologic, France) at 25 °C.

3. Results and discussion

It is well known [13–15] that the olivine LFP can be only obtained in an inert or reductive atmosphere to prevent the Fe(II) from oxidizing to Fe(III). On another hand, the spinel LMN is usually calcinated in air or under O_2 to keep the Mn at higher valence [2,19]. In this work, we first tried to prepare LFP-coated LMN in Ar at 700 °C. Unfortunately, only Mn_3O_4, $(Fe,Ni)_3P$ and small amount of Li_3PO_4 were detected in the XRD pattern of the final product (not shown here). No LFP or LMN was obtained using the sol–gel method in Ar. Apparently, the Mn (IV) in LMN was reduced to Mn (III) in Ar, and the Fe (II) was oxidized to Fe (III). Therefore, it is nearly impossible to prepare the LFP-coated LMN using a sol-gel method, which needs a heat-treatment in an inert or reductive atmosphere.

Therefore, we tried a novel mechano-fusion dry process by directly mixing the commercial carbon-coated LFP and LMN without any further annealing. During mechano-fusion, nano-sized C-LFP (guest particle) is supposed to adhere to LMN (host particle) to form an enveloping shell so that the composite displays both the host and the guest properties [20]. The analysis of the XRD diagram shown in Fig. 2 confirmed that there was no structural change after mechano-fusion dry process: the XRD features associated to the LMN part remained unchanged. They are indexed in the cubic system (*Fd3m* S.G) in Fig. 2. After the mechano-fusion, the XRD spectrum simply contains the additional peaks associated to the LFP part (red marks in Fig. 2), which gives evidence that the LFP coating layer is well crystallized.

Fig. 3 compares the morphology changes before/after coating. After Fig. 3a, the LMN is made of particles 200 nm-thick. These particles agglomerate to form secondary spherical particles about ~5 μm-thick. This morphology is suited to surface coating and modification [12]. In particular, upon lamination in the manufacturing process of the batteries, the primary particles separate, so that only the size of the primary particles matters. After 20 wt% of coating, LMN surface is uniformly covered by LFP (Fig. 3b). The elemental EDX analysis of the surface layer after mechano-fusion dry process is given by the spectrum shown in Fig. 4. Most of the elements found on the surface were Fe, P, and O issuing from LFP

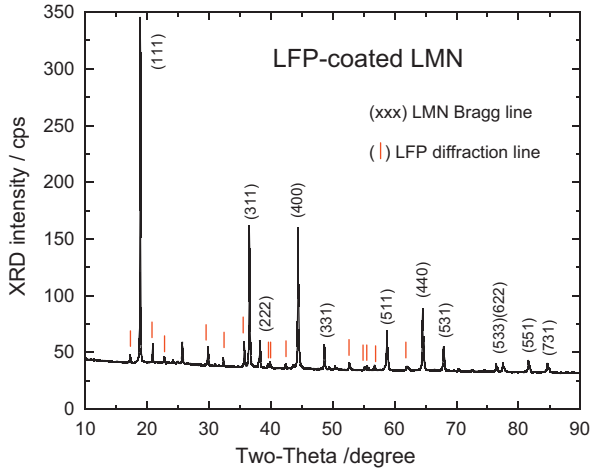

Fig. 2. XRD pattern of the C-LFP coated LMN sample obtained by mechano-fusion. The Bragg lines indexed are those of the spinel $LiMn_{1.5}Ni_{0.5}O_4$ lattice, while the main lines of the $LiFePO_4$ olivine are marked in red. No impurities were detected. (For interpretation of the references to color in this figure legend, the reader is referred to the web version of this article.)

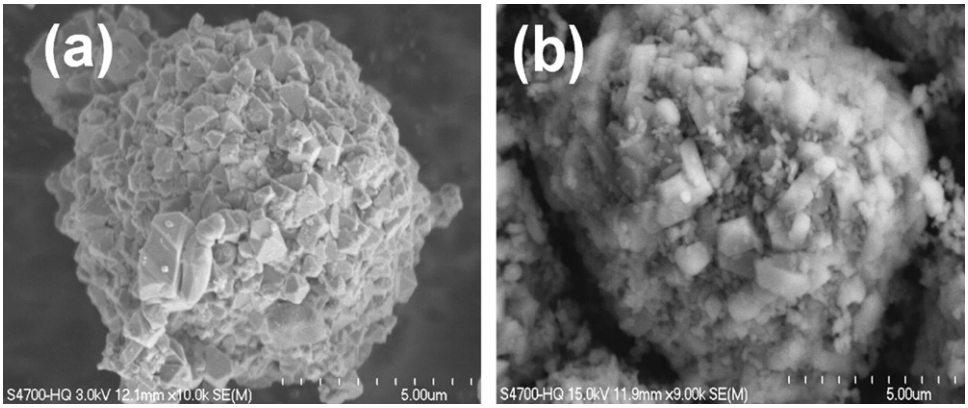

Fig. 3. SEM micrographs of the LMN (a) and LFP-coated LMN (b). After 20 wt% of coating, the LMN surface is uniformly covered by LFP.

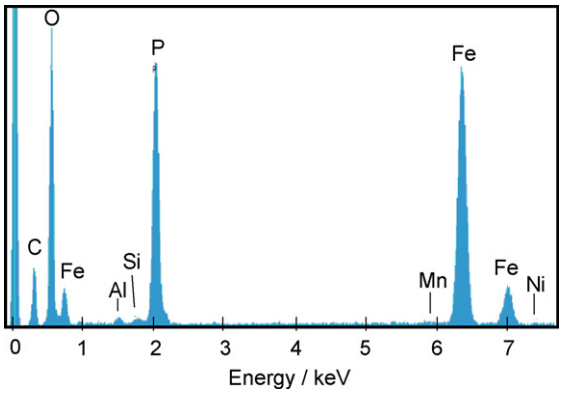

Fig. 4. Surface EDX spectrum of the LFP-coated LMN. Most of the elements found on the surface were Fe, P, and O issuing from LFP nanoparticles.

nanoparticles. Only small amounts of Mn and Ni were detected after mechano-fusion dry process, which gives evidence that LFP nanoparticles formed a uniform coating layer and covered on LMN surface, according to our illustration in Fig. 1. This is confirmed by the TEM images and EDS maps displayed in Fig. 5. The LFP is identified by both the P and the Fe elements in these maps, showing that LFP covers the whole surface of the particles. The LFP surface layer is also an attractive cathode for lithium-ion batteries at lower voltage of 3.5 V (vs. Li^+/Li^0), making it less reactive towards electrolyte with a higher electrochemical stability window [4,13].

The electrochemical properties were only carried out for the pristine LMN and LFP-coated LMN by mechano-fusion dry process. Fig. 6 compares the charge/discharge curves of the Li/LMN and Li/LFP-coated LMN coin cells for the first two cycles (cycling between 3.0 and 4.9 V at *C*/24 rate). The electrochemical results are summarized in Table 1. For the pristine LMN, only the 4.7 V voltage plateau corresponding to the Ni(IV)/Ni(II) redox reaction was observed. The Li/LMN cell delivered a reversible capacity of 104 mAh g^{-1} with coulombic efficiency (CE) of 67% and 86% for the 1st and 2nd cycles, respectively. It is interesting to note that the LFP guest is also an active cathode material, as well as a protecting layer for LMN. This is very different from the other coatings such as metal oxides or metal phosphates, which are inactive materials for LMN [16]. For the LFP-coated LMN, a similar 4.7-V plateau confirms that there is no structural change for the host LMN after mechano-fusion dry process, which is consistent with our structural analysis. In previous reports on LFP coating [16,17], no 3.5-V plateau was observed for LFP coating probably due to small amount of LFP coating (less than 5 wt%). In our work, with 20 wt% of LFP coating, the characteristic 3.5-V (Fe^{3+}/Fe^{2+}) plateau was clearly seen in Fig. 6 at low *C*-rate. A higher capacity of 123 mAh g^{-1} was obtained for the Li//LFP-coated LMN cell with *CE* of 76% and 88% for the 1st and 2nd cycles, respectively, owing to the active LFP coating.

Table 1
Electrochemical performance of the Li/LMN and Li/LFP-coated LMN cells. EC1,2, columbic efficiency for the first and second cycle, respectively; C_{Dis}, discharge capacity.

Sample	EC1 (%)	EC2 (%)	C_{Dis} (mAh g^{-1})
LFP-coated LMN	76	88	123
Pristine LMN	67	86	104

Electrochemical impedance spectroscopy (EIS) studies were performed to better understand the electrochemical performances. EIS plots of the bare and LFP-coated LMN after formation at *C*/24 and high rate tests are shown in Fig. 7. A comparable interface was obtained after formation test (Fig. 7a). However, the interface changed after high rate tests (Fig. 7b), the LFP-coated LMN showed lower lithium-ion diffusion resistance (at high frequency region) and charge transfer resistance (at medium-to-low frequency region) than that of the bare LMN. This result shows that the LFP coating can keep the LMN particles from direct contact with the electrolyte and suppress the undesired side reactions between LMN/electrolyte, therefore slowing down the SEI formation on the LMN surface. The carbon coating above the LFP layer also plays an important role. The carbon is known to allow for the much faster drain of the electrons to the collector, since the electrons have only a small path inside the LiFePO4 particle, before they are drained to the collector through the percolating conducting carbon. This faster move of the electrons toward the collector also allows for the faster move of the Li+ ions across the electrolyte without impairing the local charge neutrality, i.e. without generating a Coulomb potential opposing the ionic motion. Therefore, the carbon has a positive effect not only on the electron kinetics, but also on the lithium insertion/extraction, by increasing the conductivity of the cathode and reducing the charge transfer resistance. Therefore, both the LFP coat and the carbon coat should be responsible for the improved rate property of the LFP-coated LMN.

The drastic reduction of the impedance after the Ragone test reported below comes from the penetration of the electrolyte into the LFP-coated LMN powder during the first cycles, which increases the effective surface area of the solid/electrolyte interface. In addition, upon cycling, the contraction/dilatation of the particles is expected to leave some defects or cracks in the carbon layer, as pathways to be permeable for lithium-ions, thus increasing the ionic conductivity [21].

Ragone tests were carried out to investigate the rate capabilities of the bare and LFP-coated LMN. Results are displayed in Fig. 8. The LFP-coated LMN exhibited better rate property than that of the

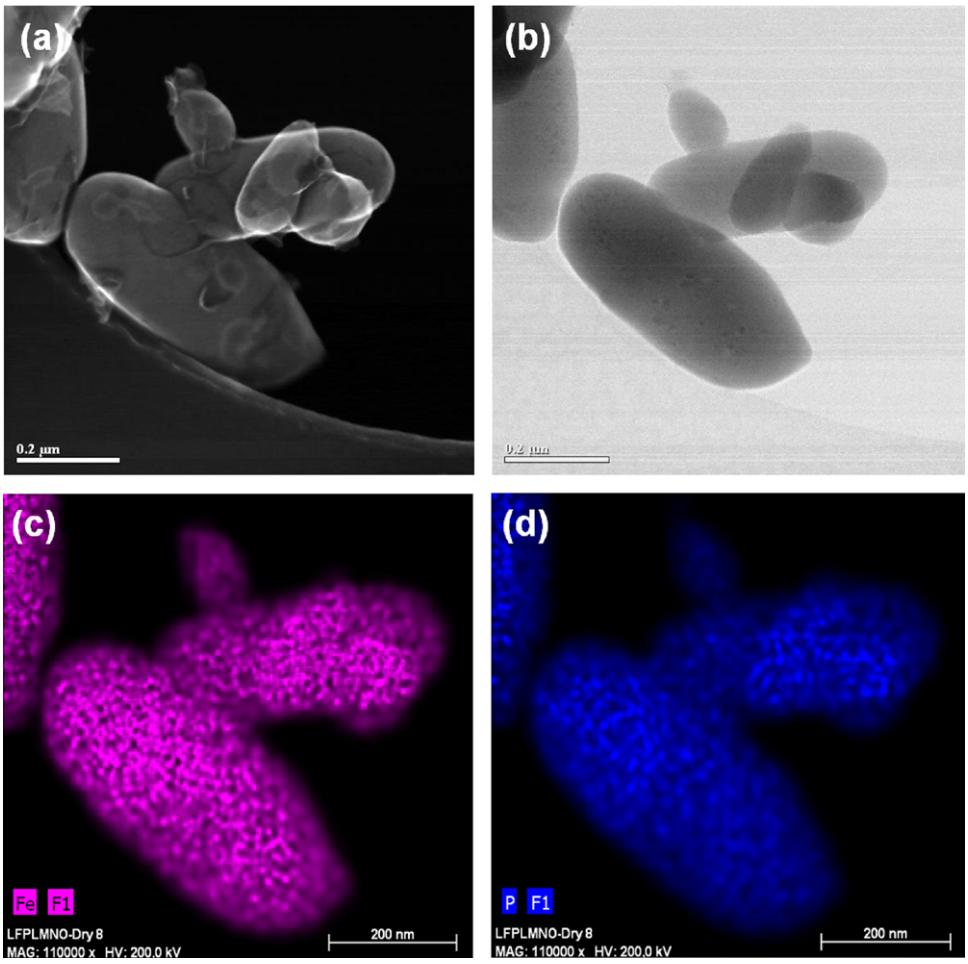

Fig. 5. TEM images (a and b) and EDX maps of P (c) and Fe (d) elements for the LMN particles coated by LFP using the mechano-fusion dry process with the LFP:LMN mass ratio is equal to 20:80.

bare LMN, especially at high rate (>10*C*), as it can be seen in Fig. 8 in the region marked with the accolade. While the bare LMN discharge capacity decreased from ~40 mAh g^{-1} at 15*C* to less than 10 mAh g^{-1} at 20*C*, LFP-coated LMN still delivered ~60 mAh g^{-1} at 15*C* and about 55 mAh g^{-1} at 20*C*. The discharge voltage profiles of the bare LNM and LFP-coated LMN between 3.0 and 4.9 V are shown in Fig. 9. At *C*-rate slower than *C*/2, the plateau of Fe^{2+}/Fe^{3+} at 3.4 V is well observed, so that the LMN contribution and the LFP

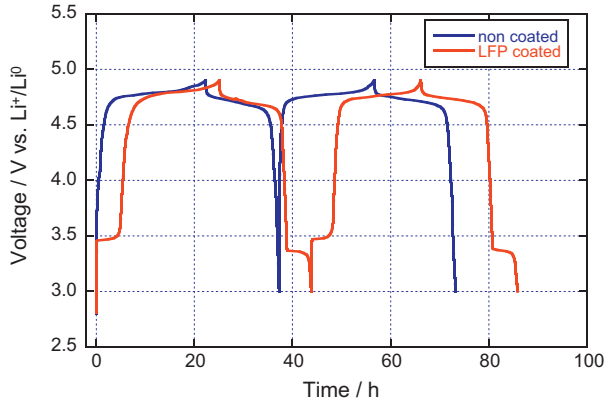

Fig. 6. Voltage profiles of the Li//LMN and Li//LFP-coated LMN cells between 3.0 and 4.9 V vs. Li^+/Li^0 at *C*/24 rate.

contribution are well separated. At *C*/12 rate, in particular, the voltage profile in Fig. 9b in the potential range $V > 3.5$ V is just proportional to that of Fig. 9a at the same *C*-rate, in the ratio 1/0.8 that corresponds to the fraction of mass of the LMN part. In other words, the voltage profile at $V > 3.5$ V in Fig. 9b is that of the LMN part, and the curve voltage–capacity per gram of LMN is the same as the corresponding curve of Fig. 9a. This is another evidence that the LFP coating did not affect the structure of the LMP part. The remaining part at $V < 3.5$ V is thus the part due to the 20 wt% LFP part, and we find that the capacity delivered by this LFP part is 150 mAh g^{-1} of LFP, which is indeed the typical capacity expected at low *C*-rate for this material, when it is well crystallized and carbon-coated. At *C*-rates faster than *C*/2, the plateau at 3.4 V has disappeared, presumably because at these fast rates, the cell is far from thermodynamic equilibrium. Therefore, it is not possible to separate the LMN and the LFP contributions. For this purpose, however, we can estimate the capacity of the LFP part from our earlier works. The Ragone plot of LFP is known to depend on the characteristic size of the particles [14]. In the present case, the characteristic length is large compared with the 20 nm obtained by wet-milling, so that the reference is the Ragone plot obtained for LFP after jet-milling. We then assume that the capacity of the LFP part per gram of LFP at the different *C*-rates is the same as that of LFP reported in Fig. 16a in ref. [14]. It is then straightforward to subtract this part from the full capacity of the LFP-coated LMN sample, to deduce the part of the capacity due to the LMN part, which we note C_{LMN} (LFP-coated), when normalized to 1 g of LMN. We have reported in

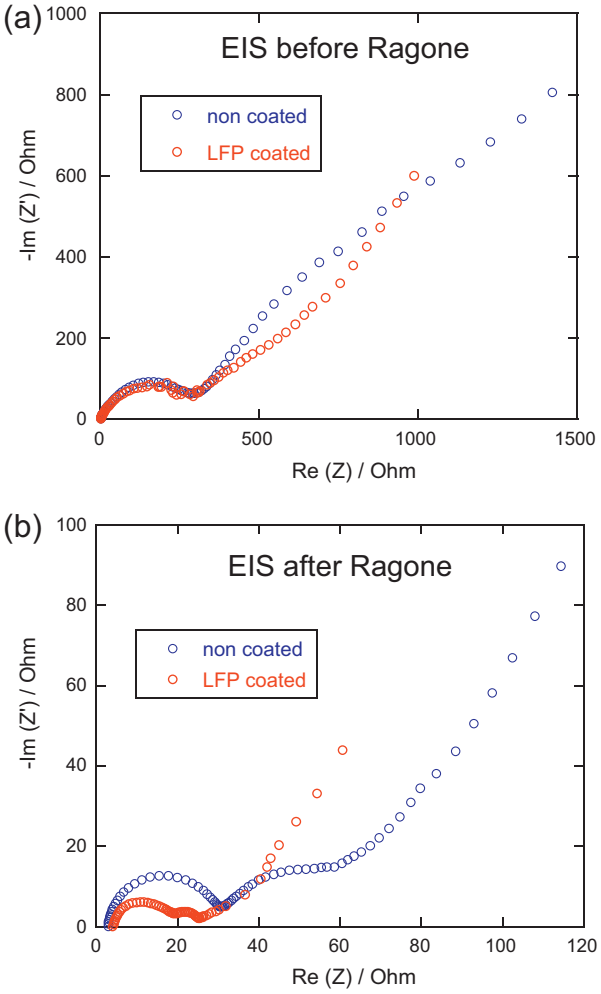

Fig. 7. EIS plots of the bare and LFP-coated LMN (a) before high rate tests (fresh cell formed at *C*/24) and (b) after high rate tests.

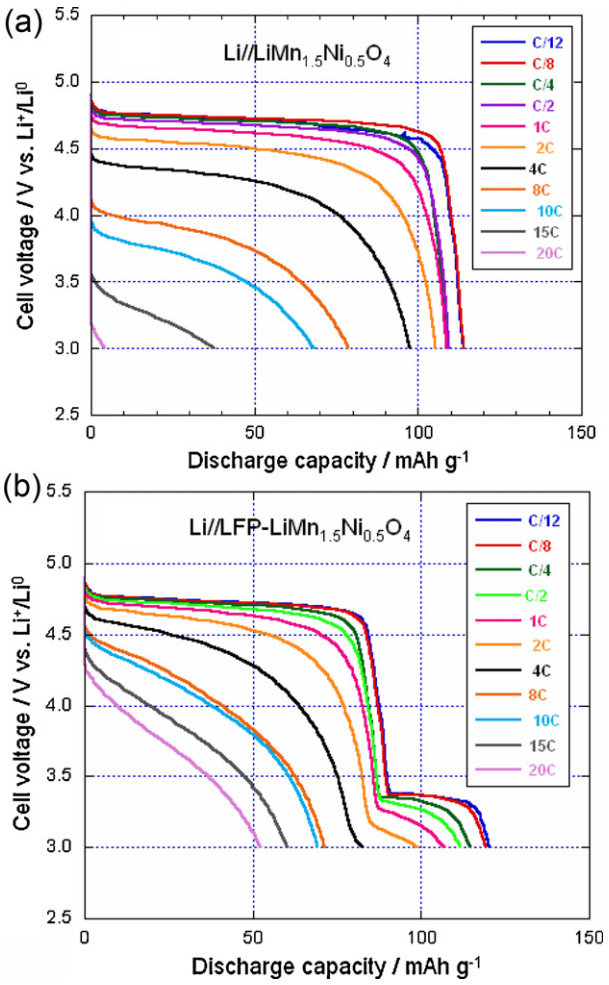

Fig. 9. Discharge profiles of the Li//LMN (a) and Li//LFP-coated LMN (b) cells at different *C* rates.

Fig. 10 the gain in capacity of the LMN part upon coating, defined as the ratio between C_{LMN} (LFP-coated) and the capacity of LMN without coating (given from Fig. 9a or in Fig. 8). We can see on Fig. 10 that the gain is just 1.0, within experimental uncertainty, at low *C*-rates, up to 10*C*. At such rates, the capacity is thus just the addition of the capacity due to the LMN part and the capacity of the LFP part. On another hand, the gain in capacity about 10*C* is increasing. It is already 1.6, meaning a 60% increase in capacity of the LMN part at 15*C*, and the gain reaches 13.3 at 20*C*. The larger capacity at such *C*-rates, evidenced in Fig. 8, is entirely due to the gain of the LMN part. This result gives evidence that the LFP part has protected the LMN part from the interaction of LMN with the electrolyte, which creates a resistive solid–electrolyte interface (SEI)

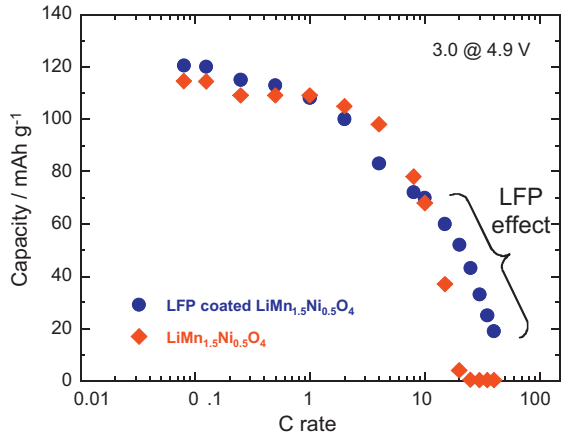

Fig. 8. Ragone plots for the Li//LMN and Li//LFP-coated LMN cells between 3.0 and 4.9 V vs. Li^+/Li^0.

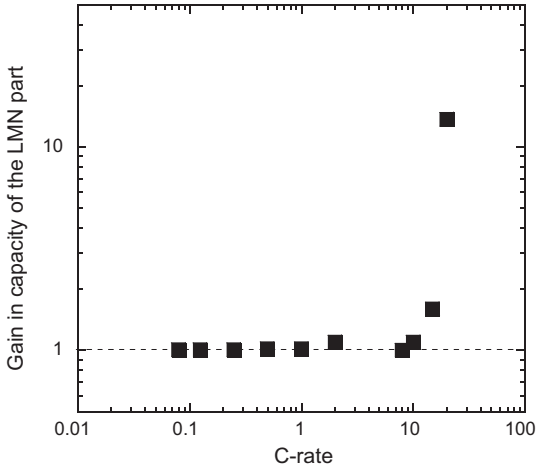

Fig. 10. Gain in capacity of the LMN part due to the LFP-coating. The gain equal to 1.0 means that the capacity of the LMN part is the same after and before LFP-coating.

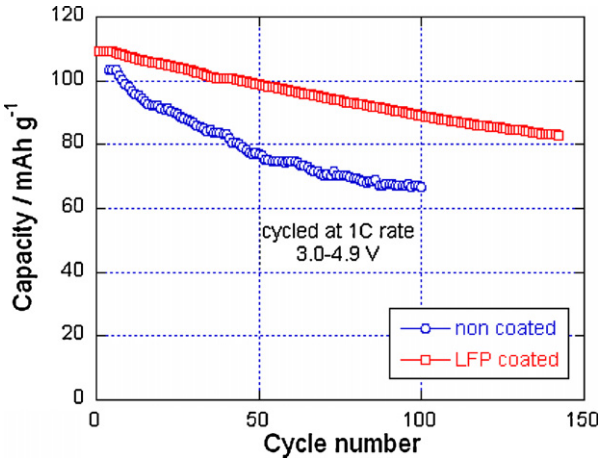

Fig. 11. Cyclability of the Li//LMN and Li//LFP-coated LMN cells at 1*C* between 3.0 and 4.9 V vs. Li^+/Li^0.

that reduces the performance of LMN at high *C*-rates. Sun et al. [9] suggested that Mn dissolution and HF generated from the decomposition $LiPF_6$ salts in the electrolyte should be the reasons for the capacity loss of pristine LMN. This reaction of LMN with the electrolyte also reduces the cycling life. Fig. 11 compares the capacity retention of the pristine and LFP-coated LMN at 1*C* rate between 3.0 and 4.9 V. For the pristine LMN, the discharge capacity decreased from ~105 to 65 mAh g^{-1} in 100 cycles, only 61.5% of capacity was retained. In contrast, LFP-coated LMN still delivered a capacity of 82 mAh g^{-1} with better capacity retention of 74.5% after 140 cycles at 1*C*.

These results suggest that the LFP coating can keep the LMN particles from direct contact with the electrolyte and suppress the undesired side reactions between LMN/electrolyte, slowing down the SEI formation on the LMN surface. Moreover, the C-LFP layer increases the conductivity of the cathode. These should be responsible for the improved rate property of the LFP-coated LMN. The gain in performance at fast *C*-rate (shown in Fig. 10) also suggests faster lithium insertion/extraction kinetics across the electrode/electrolyte interface after LFP coating. On the other hand, we assume that the C-LFP protecting coat suppresses the surface rearrangement during cycling, and thus improves the cycling performance of the LMN spinel. As previously reported, LMN suffers severe capacity loss when cycled at high temperature (50–60 °C) [9,22,23], but LFP shows very good rate performance both at room temperature and 60 °C [24,25]. We expect that the LFP coating will also increase the cycling performance of the LMN at 60 °C. This work is still undergoing, the results will be discussed later.

4. Conclusion

With a novel mechano-fusion dry process, C-$LiFePO_4$-coated $LiMn_{1.5}Ni_{0.5}O_4$ composite particles were successfully synthesized. The LFP coating serves as both active cathode and protecting material, which leads to better high rate performance and improved cyclability at room temperature. The enhanced performance is due to a reduced surface-layer resistance and charge-transfer resistance. The studies demonstrate that the LFP coating should offer important benefits to increase the rate property as well as cycling performance for lithium-ion batteries.

Acknowledgments

The authors would like to acknowledge the support from the U.S. Department of Energy under the BATT program (Lawrence Berkeley National Laboratory) and Hydro-Québec.

References

[1] K. Amine, H. Tukamoto, H. Yasuda, Y. Fujita, J. Power Sources 68 (1997) 604.
[2] Q. Zhong, A. Bonakdarpour, M. Zhang, Y. Gao, J.R. Dahn, J. Electrochem. Soc. 144 (1997) 205.
[3] J.B. Goodenough, in: W. Van Schalkwijk, B. Scrosati (Eds.), Advances in Lithium-Ion Batteries, Kluwer Adademic/Plenum Publishers, New York, 2002.
[4] J. Goodenough, Y. Kim, Chem. Mater. 22 (2010) 587.
[5] D. Liu, J. Han, M. Dontigny, P. Charest, A. Guerfi, K. Zaghib, J.B. Goodenough, J. Electrochem. Soc. 157 (2010) A770.
[6] J. Liu, A. Manthiram, Chem. Mater. 21 (2009) 1695.
[7] Y.K. Sun, K.-J. Hong, J. Prakash, K. Amine, Electrochem. Commun. 4 (2002) 344.
[8] T. Noguchi, I. Yamazaki, T. Numata, M. Shirakata, J. Power Sources 174 (2007) 359.
[9] Y.K. Sun, Y.S. Lee, M. Yoshio, K. Amine, Electrochem. Solid State Lett. 5 (2002) A99.
[10] Y. Kobayashi, H. Miyashiro, K. Takei, H. Shigemura, M. Tabuchi, H. Kageyama, T. Iwahori, J. Electrochem. Soc. 150 (2003) A1577.
[11] J.Y. Shi, C.-W. Yi, K. Kim, J. Power Sources 195 (2010) 6860.
[12] H.M. Wu, I. Belharouak, A. Abouimrane, Y.-K. Sun, K. Amine, J. Power Sources 195 (2010) 2909.
[13] A.K. Padhi, K.S. Nanjundswamy, J.B. Goodenough, J. Electrochem. Soc. 144 (1997) 1188.
[14] K. Zaghib, P. Charest, M. Dontigny, A. Guerfi, M. Lagace, A. Mauger, M. Kopec, C.M. Julien, J. Power Sources 195 (2010) 8280.
[15] S. Ferrari, R. Lassarote Lavall, D. Capsoni, E. Quartarone, A. Magistris, P. Mustarelli, P. Canton, J. Phys. Chem. C 114 (2010) 12598.
[16] H. Wang, W.-D. Zhang, L.-Y. Zhu, M.-C. Chen, Solid State Ionics 178 (2007) 131.
[17] W.-S. Kim, S.-B. Kim, I.C. Jang, H.H. Lim, Y.S. Lee, J. Alloys Compd. 492 (2010) L87.
[18] K.-F. Hsu, S.-Y. Tsay, B.-J. Hwang, J. Mater. Chem. 14 (2004) 2690.
[19] B.J. Hwang, Y.W. Wu, M. Venkateswarlu, M.Y. Cheng, R. Santhanam, J. Power Sources 193 (2009) 828.
[20] M. Alonso, M. Satoh, K. Miyanami, Powder Technol. 59 (1989) 45–52.
[21] G.-N. Zhu, C.-X. Wang, Y.-Y. Xia, J. Electrochem. Soc. 158 (2011) A102.
[22] J. Liu, A. Manthiram, J. Phys. Chem. C 113 (2009) 15073.
[23] H.M. Wu, J.P. Tu, Y.F. Yuan, Y. Li, X.B. Zhao, G.S. Cao, Electrochim. Acta 50 (2005) 4104.
[24] C. Zhu, Y. Yu, L. Gu, K. Weichert, J. Maier, Angew. Chem. Int. Ed. 50 (2011) 6278.
[25] K. Zaghib, N. Ravet, M. Gauthier, F. Gendron, A. Mauger, J.B. Goodenough, C.M. Julien, J. Power Sources 163 (2006) 560.